Hindawi
Concepts in Magnetic Resonance Part B
Volume 2019, Article ID 4139726, 8 pages
https://doi.org/10.1155/2019/4139726

Research Article

Inherent Geometry Correction for Diffusion EPI Using the Reference Echoes as Navigators

Johan S. van den Brink and Jos J. Koonen

Philips MRI, Netherlands

Correspondence should be addressed to Johan S. van den Brink; johan.van.den.brink@philips.com

Received 14 March 2019; Revised 13 April 2019; Accepted 6 May 2019; Published 26 May 2019

Academic Editor: Xiaodong Yang

Diffusion-weighted EPI has become an indispensable tool in body MRI. Geometric distortions due to field inhomogeneities are more prominent at large field–of–view and require correction for comparison with T2W TSE. Several known correction methods require acquisition of additional lengthy scans, which are difficult to apply in body imaging. We implement and evaluate a geometry correction method based on the already available non phase-encoded EPI reference data used for Nyquist ghost removal. The method is shown to provide accurate and robust global geometry correction in the absence of strong, local phase offsets. It does not require additional time for calibrations and is directly compatible with parallel imaging methods. The resulting images can serve as improved starting point for additional geometry correction methods relying on feature extraction and registration.

1. Introduction

Diffusion-weighted (DW) EPI provides improved specificity in oncologic body MRI beyond T2W TSE sequences [1]. Global and local geometric distortions inherent to DW EPI often complicate diagnostic combination of DW and T2W data. These EPI artifacts result from static or dynamic field variations, which add a phase error relative to the slow phase evolution in the k_y direction, i.e., along the blip gradients [2].

Diffusion gradients induce eddy currents from which phase is accumulated during the EPI acquisition, resulting in shear, stretch and compression, and displacements in the images [3]. Compensation is provided by hardware improvements or sequence modifications to reduce the eddy currents, or by image registration approaches; for an overview see [4, 5].

Offsets and variations in the static magnetic field also cause phase accrual during the EPI acquisition. Subject-specific (higher order) shimming in the abdomen reduces field-error variance down to typically 70–100 Hz at 3T in a specific slice, while local susceptibility effects add frequency offsets up to several hundreds of Hz. Given typical bandwidths along k_y of 20–30 Hz per pixel, image distortions of 3–5 pixels (global) up to more than 10 pixels (local) are observed and require additional correction strategies.

Image distortions can be reduced significantly by SENSE [6] as it increases the bandwidth in the k_y direction, proportional to the reduction factor [7, 8]. Application of parallel imaging does not add any scan time overhead beyond coil sensitivity mapping. Another efficient method for multiple average DW EPI exploits the fact that distortions in acquisitions with reversed blip gradient polarity are equal but opposite [9–11]. The desired true signal location is derived from line integrals and edge detection [12, 13], optionally extended with elastic registration or model function fitting approaches [9, 11]. A potential disadvantage of this method, apart from the significant computation time, is that it works in final image space and thus requires accurate SENSE unfolding to precede the unwarping operation. Other approaches map the (residual) static field deviations by regular field maps [14, 15], by converting the EPI readout into a multiple gradient echo sequence to perform point-spread function (PSF) mapping [15, 16]. Apart from significant additional scan time required for the field mapping, breathing motion and patient compliance during the field map acquisition and motion between the field map and the actual DW EPI sequence make this approach difficult to implement in practice, especially for abdomen MRI.

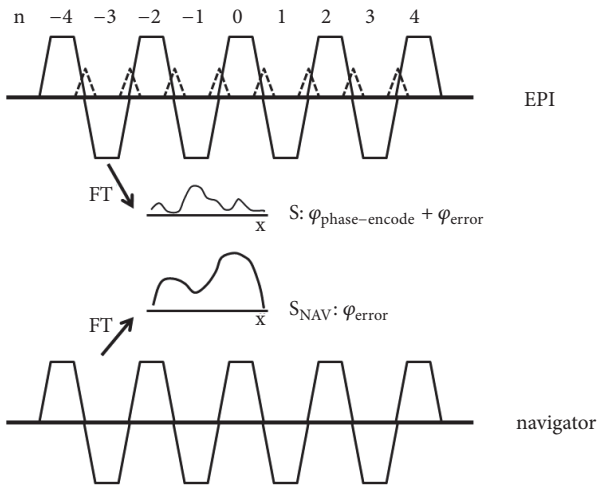

Figure 1: Schematic representation of the EPI readout with phase encoding blip gradients (top), and nonphase–encoded reference readout (bottom) used as navigator to probe the phase errors. Since both readouts are identical, each echo at index n has accumulated the same phase error in both acquisitions, which phase from the navigator can be used to recover unperturbed k-space.

The other inherent EPI artifact, the Nyquist N/2–ghost, is the result of timing differences between echoes acquired with positive and negative gradient lobes. It is normally removed by phase correction of one set of the imaging echoes by the phase difference between nonphase encoded (navigator) echoes acquired under both polarities of the readout gradient [17, 18]. For ghost removal, a subset of navigator echoes is taken from a full EPI readout without phase encoding.

It is recognized in [18] that the phase evolution from all echoes can provide a means for geometry correction. Here, we report a SENSE compatible, robust implementation of the combined EPI N/2–ghost removal and geometry correction from individual navigator echo signals. This provides an efficient and effective global geometry correction method without additional calibration time. We show that elimination of the fat fraction from the observed phase by spectral fat suppression is crucial for a practical implementation. Strong local geometry distortions are not corrected by the navigator projection technique, for which additional corrections are required, e.g., using the dual polarity phase-encode method [4, 10].

2. Theory

Without loss of generality, we consider a single-shot EPI readout traversing full k-space on an essentially rectilinear grid as indicated in Figure 1. The speed of k-space traversal is high in the readout or k_x direction and low in the phase-encode or k_y direction. As a result, distortions in the X-direction are negligible. After Fourier transform along k_x for all echoes, the 1–dimensional EPI signal for any X-location is given by

$$S\left(x,k_y\right) = \int \rho\left(x,y\right) \exp\left(i\phi_{error}\left(x,y\right)\right) \exp\left(ik_y y\right) dy \quad (1)$$

where $\rho(x, y)$ is the spin density at location (x,y), T_2^* decay is ignored, and ϕ_{error} is the total phase error. For spin echo EPI, any k_y line is sampled at an effective echo time $TE_{eff} = n\Delta t$, where Δt is the duration of a single k_x readout including the time required for the blip gradient and n the index of the k_y line, running from $-N_y/2$ to $N_y/2$ for a full k-space acquisition. ϕ_{error} can be divided into contributions that evolve with TE_{eff}, such as main field inhomogeneities, flow and motion, or residual eddy currents from diffusion gradients, and constant terms, such as variations in coil phase or gradient delay differences for odd and even k_y lines. The latter terms can be removed by known techniques [17], and we only consider ϕ_{error} from main field offsets, i.e., $\gamma B_0 TE_{eff}$. The resulting geometric distortion is then given by

$$y = y_0 + \frac{\Delta f\left(y_0\right)}{BW_{k_y}} \quad (2)$$

where y_0 is the true signal location, y the resulting image location, Δf the frequency offset at that location, and BW_Y the bandwidth per pixel in the phase-encode direction.

Correction of the geometric distortion is possible if the frequency offset can be measured. We intend to use the nonphase–encoded EPI reference echoes to measure ϕ_{error} as function of TE_{eff}, see lower trace of Figure 1. This navigator phase ϕ_{error} averages frequency offsets along the Y-direction for any X-location. The presence of multiple frequency components causes a complex evolution of this projected phase as function of TE_{eff} such that the navigator data is subject to additional requirements to obtain the desired geometry correction. Consider the obvious example of water and fat fractions with distinct frequency differences, in which case the EPI signal formula develops into

$$\begin{aligned} S\left(x,k_y\right) = \int \rho\left(x,y\right) \Big\{ & W \exp\left(2\pi i \Delta f_W\left(x,y\right) TE_{eff}\right) \\ & + (1-W) \exp\left(2\pi i \Delta f_F\left(x,y\right) TE_{eff}\right) \Big\} \\ & \cdot \exp\left(ik_y y\right) dy \end{aligned} \quad (3)$$

where $\Delta f_{W,F}$ is the frequency offset for the water fraction (W) and the fat fraction (1 − W = F), respectively. The water and fat fractions are defined by $|\Delta f_W| \leq 2$ ppm, and $|\Delta f_F| > 2$ ppm. To correct the frequency offset at any k_y line, a nonphase encoded reference scan ($k_y = 0$) is acquired with signal intensity

$$\begin{aligned} S_{NAV}\left(x\right) = \int \rho\left(x,y\right) \Big\{ & W \exp\left(2\pi i \Delta f_W\left(x,y\right) TE_{eff}\right) \\ & + (1-W) \exp\left(2\pi i \Delta f_F\left(x,y\right) TE_{eff}\right) \Big\} dy \end{aligned} \quad (4)$$

i.e., the projection of intensity-weighted phase offsets at all y–locations. As indicated in Figure 1, the phase errors are identical in the EPI and the reference readout, enabling geometry correction by subtraction of the (averaged) phase of $S_{NAV}(x)$ from $S(x, k_y)$. This approach can be applied to both single-shot and multishot EPI readouts. Note, however, that an average phase is used to correct location–dependent

phases and thus residual phase errors will be observed if the local frequency offset deviates from the average frequency probed by the navigator. An obvious source for error is the presence of a significant fat fraction with its distinct frequency offset. To prevent a "fat shift" due to the navigator correction, spectral fat suppression must be applied to the navigator echoes. The resulting navigator signal can be described with W = 1.0 and $\rho(x, y)$ replaced by the spin density of the water fraction $\rho_W(x, y)$. Similar problems of overcorrection can occur if a local susceptibility artifact or a strong flow term biases the navigator phase. Stabilization of the phase correction is achieved by capping the maximum allowed frequency offset and smoothing the correction function over x-locations.

3. Methods

3.1. Simulations. To evaluate the efficacy of the proposed geometry correction method, we use a 1–dimensional numerical phantom consisting of 3 parts: a central part with 80% water (with a residual average frequency offset of 60Hz) and 20% fat (Δf_F = 440 Hz at 3T), two equal intensity outer parts representing 100% fat, and a narrow water-only structure representing a susceptibility artifact (with a frequency offset of –100 Hz). Simulations of a 128–echo EPI readout were performed in Mathcad. The navigator phase data were applied without further processing.

3.2. Data Acquisition and Processing. All experiments were performed using a 16-channel Torso coil on a Philips Achieva 3.0T TX clinical scanner, Release 3.2, with modified reconstruction software implementing the per-echo phase correction. Volunteer scanning was performed after informed consent and according to local guidelines. Parameters for the DW EPI sequence: 375 mm (RL, 124 pixels) x 300 mm (AP, 100 pixels) x 220 mm (FH, 40 slices), TE/TR = 30/1560 ms, scan time 22 s (2 averages, single breath hold), SENSE factor 2, 70% partial Fourier, 37 EPI readouts, BW_X/BW_Y = 3660/44 Hz/pixel. SPIR fat suppression, diffusion b = 20 s/mm^2. Phase encoding directions Anterior–>Posterior (AP) and Posterior–>Anterior (PA) were acquired in separate scans. The phantom images were acquired with the same protocol, but no SENSE (i.e., 71 EPI readouts, and BW_Y = 22 Hz/pixel). Anatomical reference images were acquired using a T2W TSE sequence: 375 mm (RL, 288 pixels) x 300 mm (AP, 187 pixels) x 220 mm (FH, 40 slices), TE/TR = 80/1250 ms, scan time 50 s (3 breath holds), SENSE factor 2, 60% partial Fourier, 58 TSE readouts, BW_X = 192 Hz/pixel.

The EPI reference data is acquired without application of diffusion-encoding gradients, and the resulting data was split and in a first processing step N/2–ghost correction from the product SW was applied to align odd and even echoes, for each coil element separately. In the second pass, the phase offset per echo was calculated using combined data from all channels [19] to prevent removal of the coil phase required for SENSE reconstruction. Data vectors for each echo in the EPI train are Fourier–transformed along the k_x direction, and a modulus-weighted fit along TE_{eff} provides the phase per X-location. The modulus weighting and the use of the fitted phase prevents erroneous geometric correction in low SNR regions. We also require the phase to be smooth along the X-direction, to prevent discontinuities in the reconstructed image. In addition, we limit the maximum phase to a value equivalent to 1 ppm to prevent overcorrection from local field errors.

4. Results

Figure 2 shows simulation results of the proposed geometry correction method for a 1–dimensional numerical phantom along the phase encoding direction (black solid line). The default reconstruction is compared with the phase–correction method using full (red line in Figure 2(a)) and fat-suppressed navigator echoes (green line in Figure 2(b)). The fat-suppressed simulation (green line in Figure 2(c)) shows good global correction and residual distortion for the susceptibility artifact. The required quality of fat suppression is evaluated in Figure 2(d) for different residual fat fractions.

The effectiveness of the phase-based geometry correction is illustrated on a phantom in Figure 3. Residual field offsets result in incomplete fat suppression at the edge of the FOV. Local field variations distort the phantom and shift the (residual) fat in the image; see Figure 3(b). Application of the phase correction realigns the distortion to create the image of Figure 3(c) which is largely realigned to the TSE reference image, Figure 3(a). We note that the lower line of the phantom is distorted by the correction with the average phase.

Figure 4 shows the results of the correction method for diffusion-weighted EPI in the abdomen. We compare EPI acquisitions with opposite phase encoding directions, Figures 4(a) and 4(c), to better demonstrate the geometric distortions relative to the T2W TSE image, Figure 4(g). Geometry correction is shown for one phase encoding direction in Figure 4(e), corresponding to the distorted image in Figure 4(c). The effectiveness of the correction is better appreciated from the zoomed images at the location of the left kidney, with lines added as guide for the eye: Figures 4(b) and 4(d) show the shifted locations of the posterior kidney wall, relative to the TSE reference image in Figure 4(h). The guiding lines for each of these images are copied onto the phase-corrected image in Figure 4(f), showing that the corrected location of the kidney closely matches that of the reference, approaching the middle of the two EPI locations.

As shown in Figure 2, structures with field offsets opposite to the average field offset as estimated from the phase of the navigator echo will not be corrected or move into the wrong direction. Figure 5 illustrates this effect for a slice where the lung-liver interface induces strong local field variations. Compression and stretching of the liver is clearly observed in Figures 5(a) and 5(c). Starting from Figure 5(a), the corrected image is shown in Figure 5(b), and Figure 5(c) shows that overall appearance of the outline of the body improves, but the stretched liver is not corrected, and its location remains obviously wrong.

5. Discussion

EPI geometry correction using full characterization of the spatial frequency offset has been investigated by several

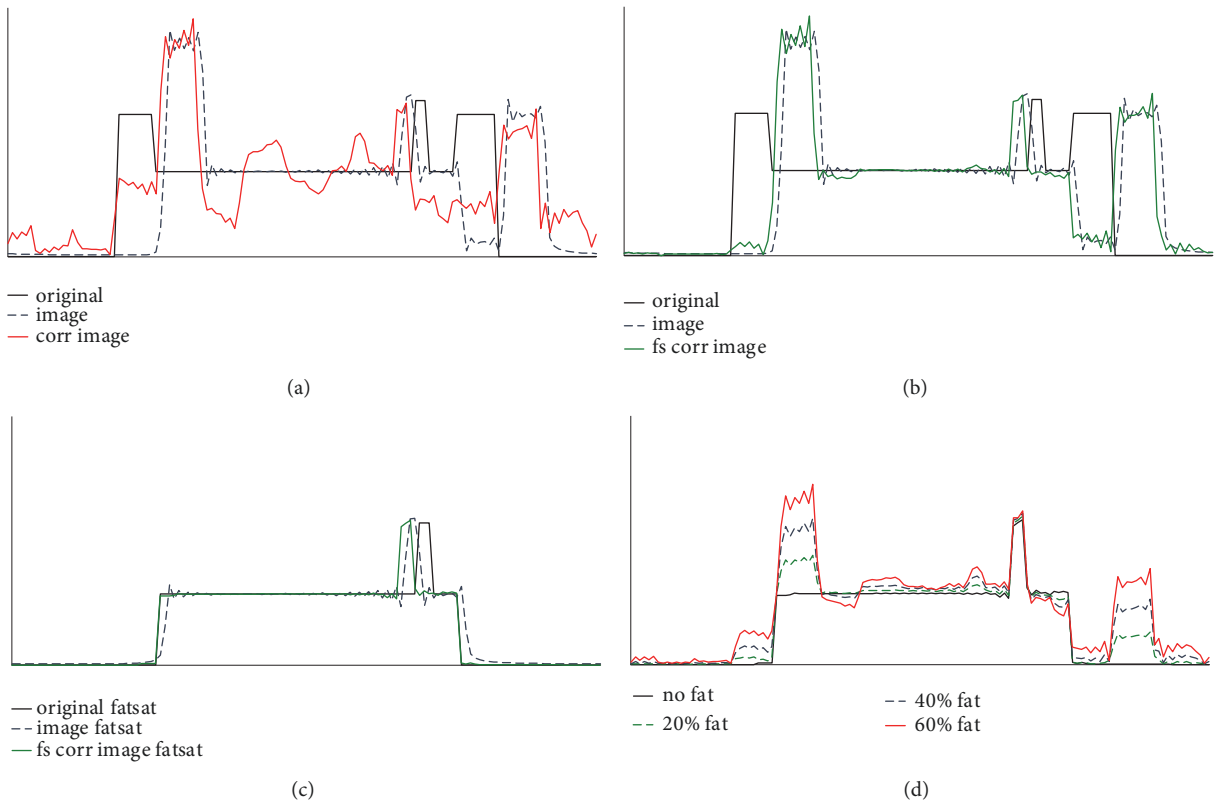

FIGURE 2: Simulations of the geometry correction using the time-dependent phase from the nonphase–encoded EPI reference scan. A 1-dimensional numerical phantom along the phase-encode direction is used, containing 3 fractions: fat rims, central composite water/fat, and a local intense water compartment with additional frequency offset. Simulations show the effect of phase correction without (a) and with (b) fat suppression for the phase correction vectors. The black solid line represents the numerical phantom, the blue dashed line represents the state-of-the-art EPI reconstruction, and the red and green solid lines shows the reconstruction where each echo is corrected with the nonphase–encoded navigator echo at the corresponding time point in the EPI train. Correction for the fat-suppressed image data is shown in (c). The sensitivity of the correction to residual fat signal is evaluated in (d) for 0% (black), 20% (green), 40% (blue), and 60% (red) residual fat signal in navigator and image.

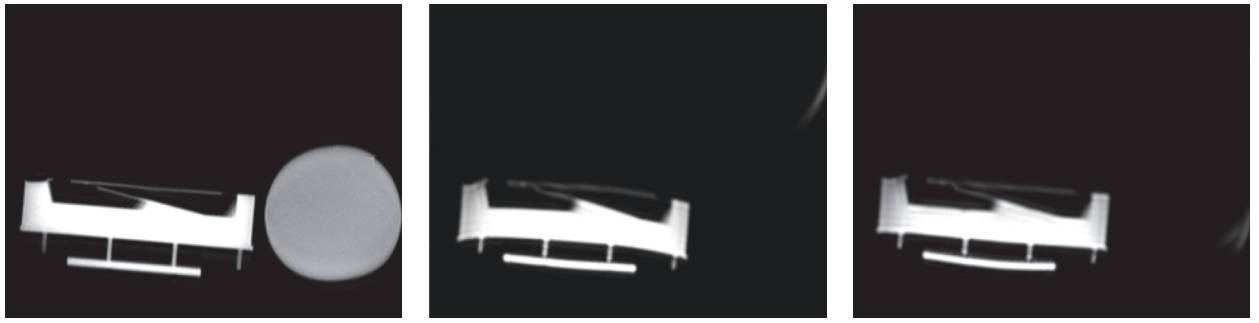

FIGURE 3: 3T T2W TSE (a) and fat-suppressed diffusion EPI images (phase shift direction P) from the manufacturer's head phantom (25 cm diameter) and a bottle filled with oil. The setup has strong local field gradients, resulting in significant EPI distortions (b) that are corrected (c) by echo–by–echo phase subtraction using the nonphase–encoded navigator echoes.

authors. The significant additional scan time required for such methods make them incompatible with abdominal imaging requirements. We investigate the possibility of implementing geometry correction based on EPI reference data as used for N/2–ghost removal [18].

Simulation shows that geometry correction is possible when fat-suppressed reference echoes are used (Figure 2). In Figure 2(a), the black solid line represents the input, which transforms into the image given by the dashed line, showing the water-fat shift, and a shift of the local susceptibility artifact

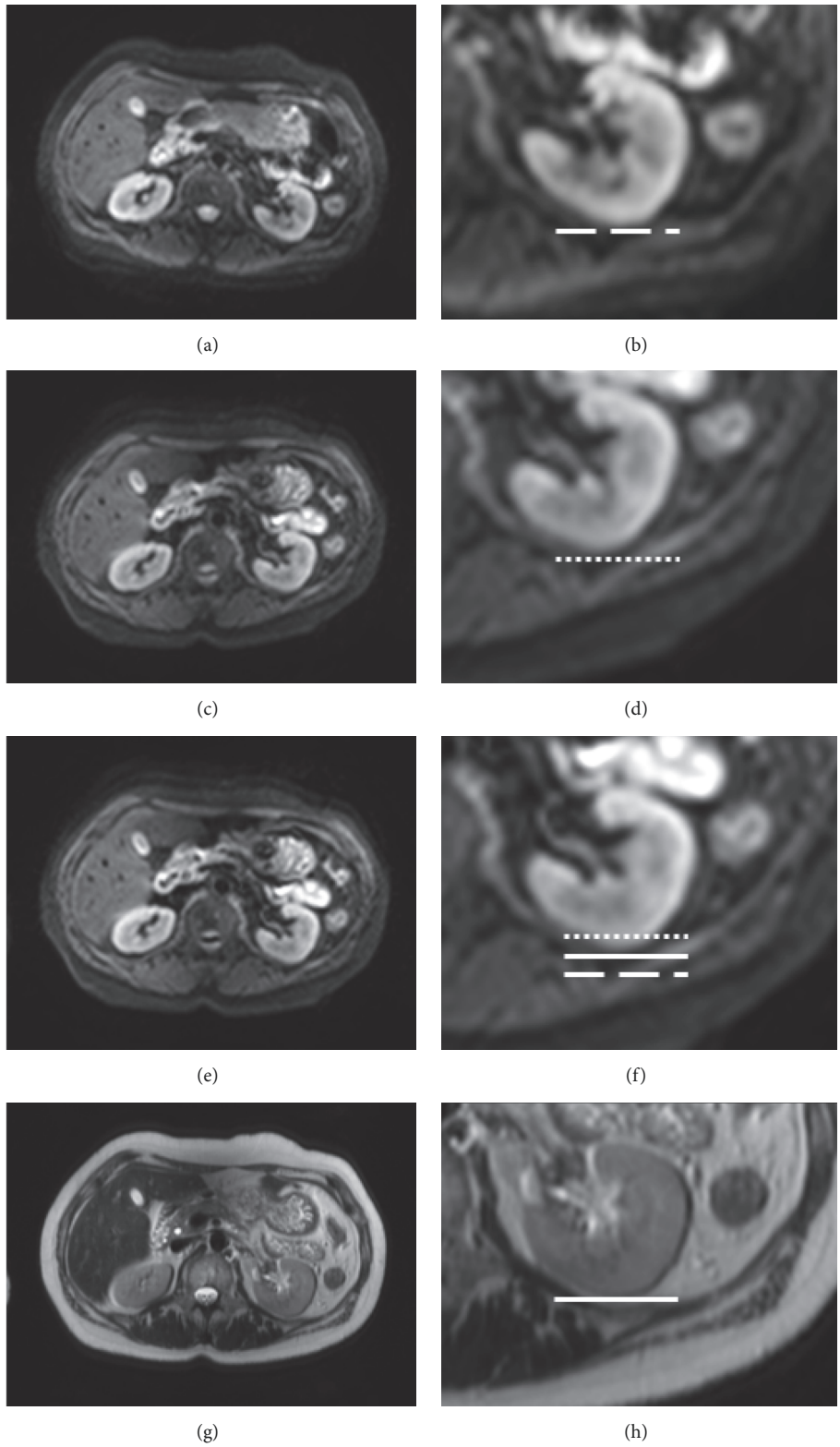

Figure 4: 3T diffusion EPI abdominal images at the level of the kidneys to demonstrate the effect of the polarity of the phase encoding gradients, and the effect of geometry correction using the phase of the navigator echoes: (a) phase shift direction A, product reconstruction, and zoomed view (b); (c) and (d) product reconstruction for phase shift direction P; (e) and (f) phase-corrected reconstruction for phase shift direction P. For reference, (g) and (h) show the (zoomed) T2W TSE image at the same location. Lines in the zoomed images indicate the edge of the kidney for the phase encoding directions A (dotted) and P (dashed) and for the T2W TSE scan (solid). Note that the phase-corrected reconstruction moves the edge position towards the middle of the A and the P EPI images, closely resembling the reference T2W TSE image data.

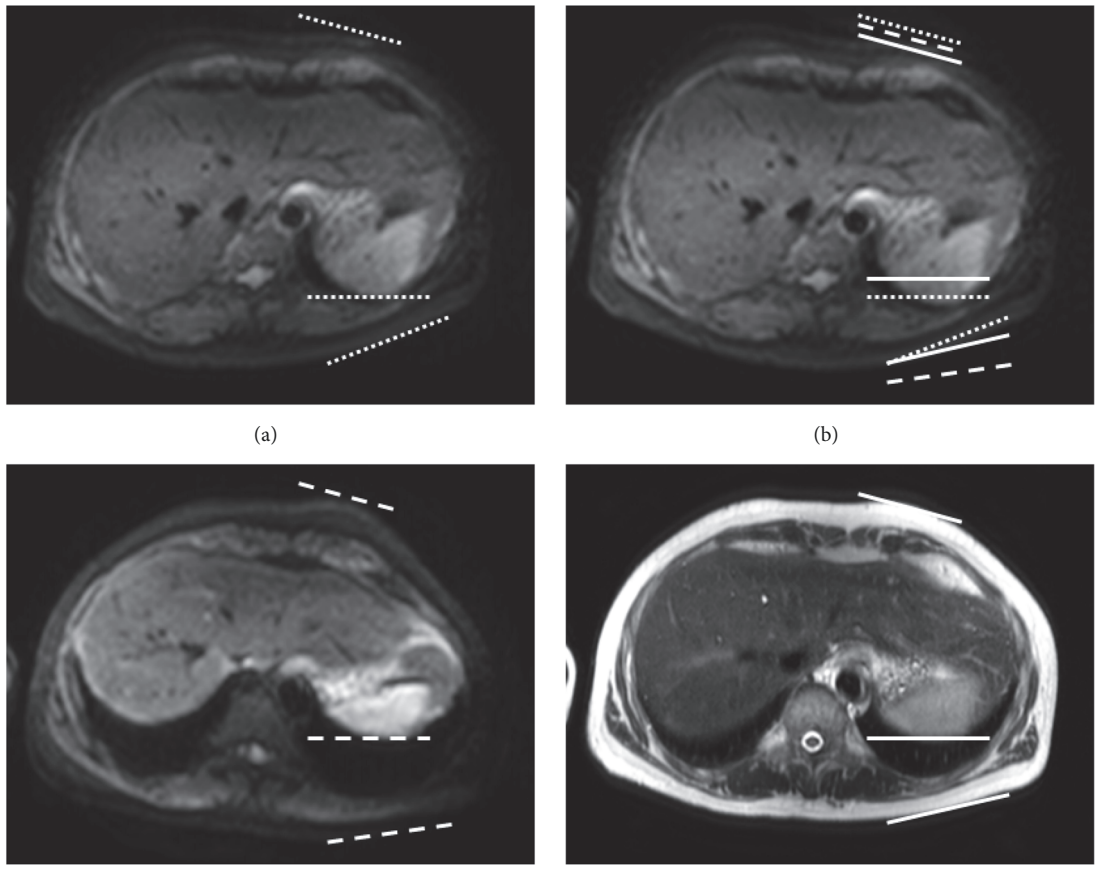

Figure 5: 3T diffusion EPI abdominal images at the lung-liver interface to show the effect of local frequency offsets opposite to the average phase as probed by the navigator: (a) phase shift direction P, product reconstruction, (b) phase shift direction P, phase-corrected reconstruction, (c) phase shift direction A, product reconstruction, and (d) T2W TSE. Lines are provided as guide for the eye to compare geometric distortions for the phase encoding directions P (dashed) and A (dotted) and for the T2W TSE scan (solid). The corrected image improves overall geometric fidelity, while the internal structures are severely distorted by the local susceptibility differences at the lung-liver interface, and the correction increases the geometric error for the position of the liver, which can be understood from the simulations in Figure 1 if the local frequency offset has opposite sign to the average frequency offset.

into the opposite direction. The red solid line is the result of phase correction using the navigator with water and fat components. The presence of multiple frequency components causes complex phase variations per EPI echo, resulting in a bad reconstruction. Removal of the fat component from the navigator phase (simulating perfect spectral fat suppression) results in a well-conditioned image as shown by the green solid line in Figure 2(b). The phase of the main water component dominates the measured average phase, and correction shifts the water part of the image back to its original location. Note that a fat-suppressed phase correction vector is applied to the nonfat-suppressed image with geometry corrections for both water and fat. The displacement of the susceptibility artifact, however, is increased by the phase correction since the measured average phase as applied for correction and the frequency offset for the artifact have the same sign. Finally, the correction method is relatively insensitive to incomplete fat suppression, with reasonable results for residual fat signals up to 20%.

The per-echo phase correction considerably improves geometric accuracy on phantoms. If only fat is present at a given X-location, the water-fat shift is compensated (Figure 3(c)). Overall improvements are observed in the head phantom part of the image, with some remaining imperfections at the edges. Geometry correction apparently can tolerate spatial averaging along the Y-direction, inherent to the use of 1–dimensional phase projections. Note, however, the bending of the narrow line at the bottom of the phantom, which is introduced by the correction method based on average phase.

The *in vivo* results corroborate the finding that average phase represents much of the residual geometric distortions when good shimming is applied. Figure 4 shows that the corrected location of features in the image shifts to the location in the anatomical reference image, being the middle of the EPI images with opposite geometric distortions. If local field inhomogeneities are present exceeding the average value, their resulting distortions are not compensated. The resulting

image will show the characteristics of the uncorrected image; see the distorted liver in Figure 5. In addition, the correction will shift small features with frequency offsets of opposite sign relative to the average further away from their true location. This calls for further correction using the reverse gradient method [9–12] to further correct distortions at locations where the average phase is determined by a small intense structure with an excessive frequency offset. The phase correction described in this work moves pixel locations based on an average field error. Implementation of a B0 field–map based geometry correction step will require compensation of the distortion field by the average accordingly.

Local overcorrection can corrupt the global image appearance, which we prevent by applying a threshold for the allowed average frequency offset (< 1 ppm) and requiring a smooth compensation function in the X-direction. With these measures, phase correction of the EPI echoes using the nonphase–encoded reference data is an obvious first step to improve the geometric accuracy of EPI images, taking full advantage of the already acquired N/2–ghost removal calibration data. Geometry correction is applied for the folded images and may reduce SENSE ghosting by an improved match between coil sensitivity calibration data and folded images.

6. Conclusions

We have demonstrated that a first step in EPI geometry correction can be achieved using the echo time-dependent phase of the EPI reference data normally used for N/2–ghost removal. The method does not require additional calibration scans, and it corrects phase in k-space which makes it processing efficient and SENSE compatible. The inherent 1–dimensional nature of the phase used for correction cannot correct for residual artifacts from local field variations. Further processing using the reversed gradient method can address those artifacts.

Data Availability

The data used to support the findings of this study are available from the corresponding author upon request.

Conflicts of Interest

Both authors are employees of Philips.

Acknowledgments

The authors thank Dr. Gwen Herigault for help with volunteer scanning. This work was funded by the EUREKA Cluster Programme ITEA, projects MEDIATE (09039) and STARLIT (16016). This work has also been presented at the ISMRM conference in 2011 [20].

References

[1] T. C. Kwee, T. Takahara, R. Ochiai, R. A. J. Nievelstein, and P. R. Luijten, "Diffusion-weighted whole-body imaging with background body signal suppression (DWIBS): features and potential applications in oncology," *European Radiology*, vol. 18, no. 9, pp. 1937–1952, 2008.

[2] F. Schmitt, M. K. Stehling, and R. Turner, Eds., *Echo-Planar Imaging: Theory, Technique and Application*, Springer Berlin Heidelberg, Heidelberg, Germany, 1998.

[3] P. Jezzard, A. S. Barnett, and C. Pierpaoli, "Characterization of and correction for eddy current artifacts in echo planar diffusion imaging," *Magnetic Resonance in Medicine*, vol. 39, no. 5, pp. 801–812, 1998.

[4] D. Jones, Ed., *Diffusion MRI*, Oxford University Press, Oxford, UK, 2010.

[5] W. Wu and K. L. Miller, "Image formation in diffusion MRI: a review of recent technical developments," *Journal of Magnetic Resonance Imaging*, vol. 46, no. 3, pp. 646–662, 2017.

[6] K. P. Pruessmann, M. Weiger, M. B. Scheidegger, and P. Boesiger, "SENSE: sensitivity encoding for fast MRI," *Magnetic Resonance in Medicine*, vol. 42, no. 5, pp. 952–962, 1999.

[7] R. Bammer, R. Stollberger, HP. Hartung, and F. Fazekas, "Parallel imaging strategies for reduction of resonance offset induced artifacts and k space filtering effects," in *Proceedings of the 8th Annual Meeting of ISMRM*, Denver, Colo, USA, 2000.

[8] T.-K. Truong, B. Chen, and A. W. Song, "Integrated SENSE DTI with correction of susceptibility- and eddy current-induced geometric distortions," *NeuroImage*, vol. 40, no. 1, pp. 53–58, 2008.

[9] J. L. R. Andersson, S. Skare, and J. Ashburner, "How to correct susceptibility distortions in spin-echo echo-planar images: application to diffusion tensor imaging," *NeuroImage*, vol. 20, no. 2, pp. 870–888, 2003.

[10] P. S. Morgan, R. W. Bowtell, D. J. O. McIntyre, and B. S. Worthington, "Correction of spatial distortion in EPI due to inhomogeneous static magnetic fields using the reversed gradient method," *Journal of Magnetic Resonance Imaging*, vol. 19, no. 4, pp. 499–507, 2004.

[11] D. Holland, J. M. Kuperman, and A. M. Dale, "Efficient correction of inhomogeneous static magnetic field-induced distortion in echo planar imaging," *NeuroImage*, vol. 50, no. 1, pp. 175–183, 2010.

[12] H. Chang and J. M. Fitzpatrick, "A technique for accurate magnetic resonance imaging in the presence of field inhomogeneities," *IEEE Transactions on Medical Imaging*, vol. 11, no. 3, pp. 319–329, 1992.

[13] S. A. R. Kannengießer, Y. Wang, and E. M. Haacke, "Geometric distortion correction in gradient-echo imaging by use of dynamic time warping," *Magnetic Resonance in Medicine*, vol. 42, no. 3, pp. 585–590, 1999.

[14] P. Jezzard and R. S. Balaban, "Correction for geometric distortion in echo planar images from B0 field variations," *Magnetic Resonance in Medicine*, vol. 34, no. 1, pp. 65–73, 1995.

[15] H. Zeng and R. T. Constable, "Image distortion correction in EPI: comparison of field mapping with point spread function mapping," *Magnetic Resonance in Medicine*, vol. 48, no. 1, pp. 137–146, 2002.

[16] M. Zaitsev, J. Hennig, and O. Speck, "Point spread function mapping with parallel imaging techniques and high acceleration factors: fast, robust, and flexible method for echo-planar imaging distortion correction," *Magnetic Resonance in Medicine*, vol. 52, no. 5, pp. 1156–1166, 2004.

[17] H. Bruder, H. Fischer, H. E. Reinfelder, and F. Schmitt, "Image reconstruction for echo planar imaging with nonequidistant k-space sampling," *Magnetic Resonance in Medicine*, vol. 23, no. 2, pp. 311–323, 1992.

[18] F. Schmitt and G. Goertler, "Method for suppressing image artifacts in a magnetic resonance imaging apparatus," *US Patent*, Article ID 5138259, 1992.

[19] F. Huang, S. Vijayakumar, Y. Li, S. Hertel, and G. R. Duensing, "A software channel compression technique for faster reconstruction with many channels," *Magnetic Resonance Imaging*, vol. 26, no. 1, pp. 133–141, 2008.

[20] A-S. Glantenay, C. J. Den Harder, J. S. Van Den Brink, G. Herigault, and J. J. Koonen, "Efficient EPI distortion correction using non-phase encoded reference data," in *Proceedings of the International Society for Magnetic Resonance in Medicine*, vol. 846, 2011.